Transient Stability Analysis and Enhanced Control of Dual-Grid-Forming MMC Under AC Grid Faults

Kaidong Lu, Zhen He, *Member, IEEE*, Junchao Ma, Chenxu Wang, Jianing Liu, Bin Hu, *Member, IEEE*, Xudong Huang, and Heng Nian, *Senior Member, IEEE*

***Abstract*—The dual-grid-forming (DGFM) control of the modular multilevel converter (MMC) can provide active power support by releasing submodule (SM) energy. At the same time, it maintains the ability to regulate dc voltage, making it promising for large-scale offshore wind power integrated high-voltage direct current systems. However, DGFM MMC are prone to transient stability problems under ac grid faults. To address this problem, a comprehensive analysis is conducted in this article to explore the transient instability mechanism of the existing DGFM MMC under ac grid faults. It is found that the interaction between SM energy control and power angle generation negatively impacts the transient stability of DGFM MMC under grid fault conditions. Based on this, this article proposes a transient stability enhanced control, which decouples power angle generation from SM energy control. With the proposed control, the transient stability of DGFM MMC is largely improved while the active power support capability is not affected. Furthermore, a root locus-based optimization method is proposed for the control parameters tuning, which can balance transient stability and active power support. Finally, the proposed transient stability enhanced control for DGFM MMC is verified with experimental results.**

***Index Terms*—AC grid faults, active power support, dual-grid-forming (DGFM) control, modular multilevel converter (MMC), transient stability.**

I. Introduction

UNDER the global trend of environmental protection and low-carbon development [1], [2], offshore wind power has experienced fast growth [3]. Currently, the mainstream integration of large capacity offshore wind power includes high-voltage direct current (HVDC) transmission, low-frequency alternative current transmission, and power frequency ac transmission [4], [5]. Among these, modular multilevel converter (MMC) based HVDC technology has been extensively adopted due to its advantages of low power loss, flexible controllability, and high reliability, e.g., the Rudong Project in China and the BorWin 2 project in Germany [6], [7].

However, the large-scale integration of offshore wind power will significantly reduce the proportion of synchronous generators in onshore power grids, thereby weakening the system's equivalent inertia and substantially increasing the burden on frequency regulation [8]. Both the 2019 U.K. "8·9" blackout incident [9] and the 2016 South Australia "9.28" blackout incident [10] are closely related to the declining inertia in these regions [11], [12].

To enhance the frequency regulation capacity of the onshore power grid, researchers are focusing on the grid-forming control of onshore MMC [13], [14], [15]. Huang et al. [13] point out that the use of grid-forming control without phase-locked loop can reduce oscillation risk. Shi et al. [14] present a grid-forming control method for MMC to operate in weak ac grids, which provides better frequency support than grid-following control. In addition, an active power support method based on grid-forming control is proposed in [15], which uses MMC submodule (SM) to enhance the active power support capacity. In a word, the existing grid-forming controls of MMC have largely improved the active power support capacity to the ac grid. However, since the ac/dc terminal voltages of MMC are strongly coupled with the SM capacitor voltage [15], the existing grid-forming controls will result in unignorable dc bus voltage fluctuations during active power supporting.

In offshore wind power integrated MMC-HVDC system, the onshore MMC is usually responsible for regulating the dc-link voltage [16]. Considering the strong demand for ac-side grid-forming, much attention has been paid to the dual-grid-forming (DGFM) control of MMC, which aims to achieve two functions simultaneously, viz., dc voltage regulation and ac voltage grid-forming. Samimi et al. [17] show that the common-mode arm voltage of MMC can be independently controlled, increasing the converter's control degrees. Building on this, Jiang et al. [18] and Kim et al. [19] propose a DGFM control method that decouples SM voltage from dc bus voltage by using the control freedom of common-mode arm voltage. Furthermore, a point of common coupling (PCC) frequency droop control that utilizes the energy of the SM is proposed, which can significantly improve the frequency performance of the ac grid through active power support [20].

Received 17 July 2025; revised 23 October 2025; accepted 16 November 2025. Date of publication 24 November 2025; date of current version 25 February 2026. This work was supported by the State Grid Zhejiang Electric Power Co., Ltd. Science and Technology Project under Grant B311DS24001B. Recommended for publication by Associate Editor M. Ordonez. *(Corresponding author: Zhen He.)*

Kaidong Lu, Zhen He, Bin Hu, Xudong Huang, and Heng Nian are with the College of Electrical Engineering, Zhejiang University, Hangzhou 310027, China (e-mail: 12310029@zju.edu.cn; hz@zju.edu.cn; binhuee@zju.edu.cn; 12310034@zju.edu.cn; nianheng@zju.edu.cn).

Junchao Ma, Chenxu Wang, and Jianing Liu are with State Grid Zhejiang Electric Power Company Ltd. Research Institute, Hangzhou 310014, China (e-mail: mjc_zjj@zuaa.zju.edu.cn; wangchenxu@whu.edu.cn; ljn94@zju.edu.cn).

Color versions of one or more figures in this article are available at https://doi.org/10.1109/TPEL.2025.3636210.

Digital Object Identifier 10.1109/TPEL.2025.3636210

Maintaining transient stability under grid faults is critically important for grid-forming converters. In general, the grid faults can be classified into two types, viz., the shallow and deep grid faults. Shallow grid faults are typically caused by load switching or high-resistance grounding, which are more common than deep grid faults. However, existing studies indicate that even under shallow faults, the grid-forming converters are still prone to transient instability issues [21], [22]. Therefore, the transient stability issue of the grid-forming converter under shallow grid fault becomes the research of this article. Shen et al. [23] reveal that maintaining the ac voltage through grid-forming control affects the dc bus voltage, which further weakens the converter's power transmission capability. Poulose and Kim [24] indicate that the grid-forming converter's operating point and control strategy affect the dc side dynamics, which may cause power oscillations. Sun et al. [25] notes that insufficient damping of the power electronic converters during frequency regulation results in transient instability under ac faults. Zhou et al. [26] points out that when power electronic converters provide active frequency support, excessive support intensity may also lead to transient system instability.

Compared with general power electronic converters, DGFM MMC has more control objectives and dimensions [19]. Therefore, during ac grid faults, the DGFM MMC can utilize additional control dimensions to enhance the system's transient stability. However, due to more complex coupling relationships, achieving both MMC active power support and transient stability becomes challenging. The challenge arises from the coupling between SM energy control and power angle generation in the DGFM MMC, which causes a delay in the power angle response and weakens transient stability.

This article concentrates on the transient stability issues of DGFM MMC under ac grid faults. The main contributions are as follows.

1) The transient stability of the existing DGFM MMC under ac faults is analyzed. The coupling relationship between transient stability and active power support capacity is revealed, providing a theoretical basis for enhancing transient stability.
2) A transient stability enhanced control method combining dc voltage branch and ac power branch is proposed, which improves the MMC power angle response speed while maintaining its active power support capability.
3) Based on the transient stability enhanced control, the linearized model of the DGFM MMC is established, and a root locus-based parameter design method is proposed to optimize the performance of the MMC under ac faults.

The rest of this article is structured as follows: in Section II, the transient stability of the existing DGFM MMC is analyzed. Section III proposes a transient stability enhanced control method, which maintains active power support capability. A root locus-based optimization method for the MMC control parameter tuning is proposed in Section IV. Section V validates the effectiveness of the proposed method with a controller hardware-in-the-loop (CHIL) experiment. Section VI concludes this article.

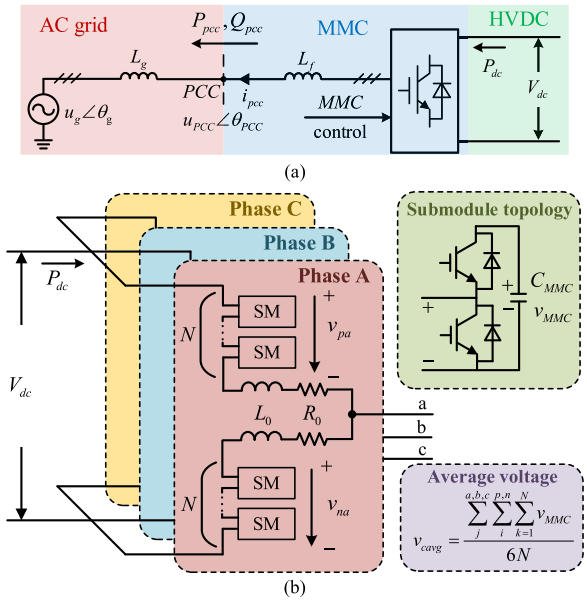

Fig. 1. Topology of MMC-HVDC system. (a) MMC-HVDC system. (b) Onshore MMC and SM.

II. Transient Stability Analysis of Existing DGFM MMC

Section II primarily introduces the topology of the MMC-HVDC system and, based on this, presents the existing control strategy for the MMC. The existing control can decouple the MMC SM capacitor from the dc bus voltage, allowing independent control of the MMC SM capacitor voltage while maintaining a constant dc bus voltage. All models and formulae in this article are expressed in per-unit (p.u.) values, with ac voltage-related parameters representing the RMS value of the phase voltage.

A. System Topology

Fig. 1(a) shows the connections of the onshore MMC. The offshore wind power is delivered to the onshore grid via MMC, represented by $P_{\rm dc}$, while the dc bus voltage is represented as $V_{\rm dc}$. L_g and L_f represent the grid inductance and the MMC filter inductance. $U_{\rm pcc}$ and $\theta_{\rm pcc}$ represent the voltage magnitude and phase angle at the PCC, while U_g ω_0 and θ_g correspond to the grid voltage magnitude and phase angle.

The topology of the MMC is illustrated in Fig. 1(b). The upper and lower arms of the MMC are each composed of N SMs. The upper and lower arm voltages are defined as v_{pj} and v_{nj} (j = a, b, c). Each SM contains a capacitor $C_{\rm MMC}$, the SM capacitor voltage is defined as $v_{\rm MMC}$. The average capacitor voltage of all the SMs in MMC is defined as $v_{\rm cavg}$. The resistance and inductance of each arm are represented by R_0 and L_0, respectively.

B. Analysis of Existing DGFM MMC

Fig. 2 depicts the existing DGFM MMC control strategy [18]. The onshore MMC needs to maintain a constant dc voltage, ensuring a stable power balance between the dc and ac grid. The

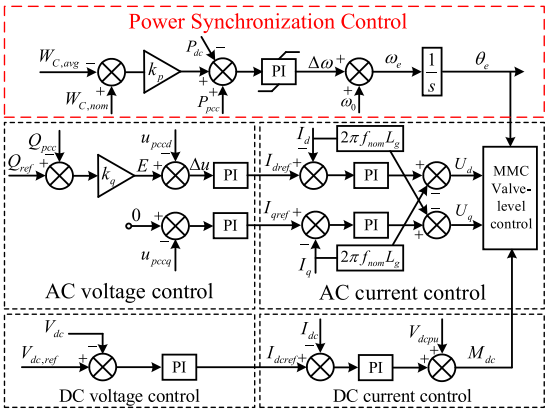

Fig. 2. Existing DGFM MMC control strategy [18].

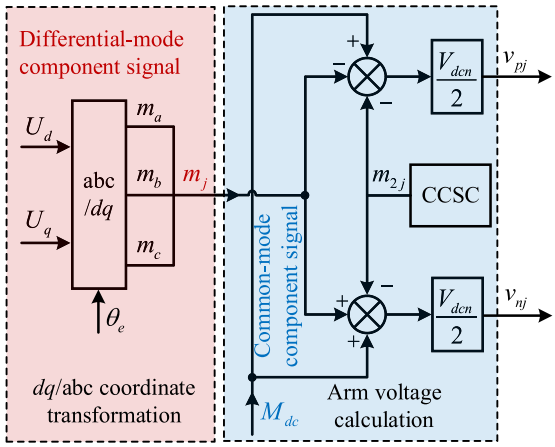

Fig. 3. MMC arm voltage calculation.

control method achieves ac/dc power balance by adjusting the power angle θ_e.

To enable independent control of the SM capacitor voltage, droop control of the SM capacitor energy is added, which is called power synchronous control. As a result, when the SM capacitor energy set value $W_{C,\mathrm{con}}$ changes, an imbalance in the ac and dc power occurs. This imbalance causes the SM capacitor to either charge or discharge, thereby adjusting its voltage. DC bus voltage is stabilized through the common-mode component M_{dc}. This method has different branches for dc voltage and capacitor voltage control, thus achieving complete decoupling between these control objectives.

The dq-axis control voltages U_d and U_q at the converter's ac port are transformed to the abc frame using the control power angle θ_e. This transformation generates the three-phase voltage modulation signals m_j (j = a,b,c), representing the per-unit values of the modulation wave voltage for each phase.

The effect of the common-mode control component M_{dc} on the arm voltage control is shown as

$$\begin{cases} v_{pj} = \frac{V_{dcn}}{2}\left(M_{dc} - m_j - m_{2j}\right) \\ v_{nj} = \frac{V_{dcn}}{2}\left(M_{dc} + m_j - m_{2j}\right) \end{cases} \tag{1}$$

where $m_{2\mathrm{j}}$ is the output of circulating current suppression control (CCSC). However, this article's analysis neglects the circulating current impact $m_{2j} = 0$ [27].

The MMC arm voltage control signal is generated by the differential-mode component m_j and the common-mode component M_{dc}. The generation method of the arm voltage control signal is shown in Fig. 3.

The DGFM control strategy decouples the SM capacitor voltage control from the dc bus voltage control (DVC) by placing them in separate control branches. However, when an ac fault occurs, the energy transmission capacity will be limited. While providing active support, the SM capacitor voltage control affects the generation of the MMC power angle.

The power angle generation branch of the existing DGFM MMC in Fig. 2 can be expressed by the following equation:

$$\omega_e = k_{pc}\int [k_p(W_{C,\mathrm{nom}} - W_{C,\mathrm{avg}}) + P_{\mathrm{pcc}} - P_{\mathrm{dc}}]dt + k_{ic}[k_p(W_{C,\mathrm{nom}} - W_{C,\mathrm{avg}}) + P_{\mathrm{pcc}} - P_{\mathrm{dc}}] + \omega_0. \tag{2}$$

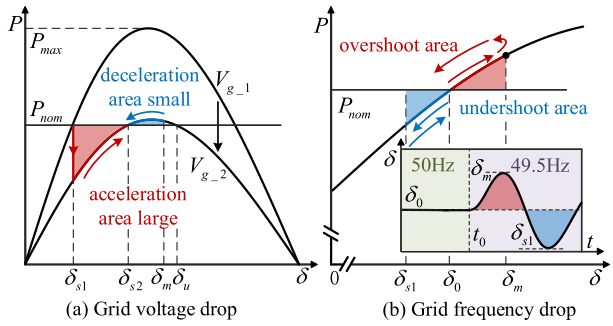

Fig. 4. Existing control method power angle curve under power grid fault. (a) Grid voltage drop. (b) Grid frequency drop.

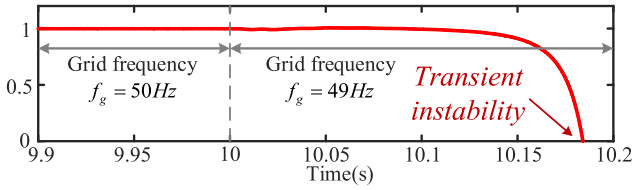

Fig. 5. Existing MMC control of power output under grid frequency drop.

When generating the power angle, the slow response of the SM capacitor energy causes a delay in the power angle response of the existing DGFM MMC. This further exacerbates the power imbalance between the ac and dc sides, potentially causing MMC instability under severe grid faults.

Fig. 4(a) shows the power angle curve under a grid voltage drop. As the voltage drops, the power angle increases from δ_{s1} to δ_{s2}, forming the acceleration area (AA). If this area exceeds the deceleration area (DA), the system loses transient stability. Fig. 4(b) shows the power angle curve under a grid frequency drop. The power angle increases from δ_0 to δ_m, with this change representing the overshoot area. The slow response of the power angle will cause large overshoot, which furtherly leads to transient instability of the MMC system.

As shown in Fig. 5, when an ac fault occurs, the coupling relationship between the SM voltage control and the power angle generation slows down the response speed of the power angle, which will cause the system output power to collapse.

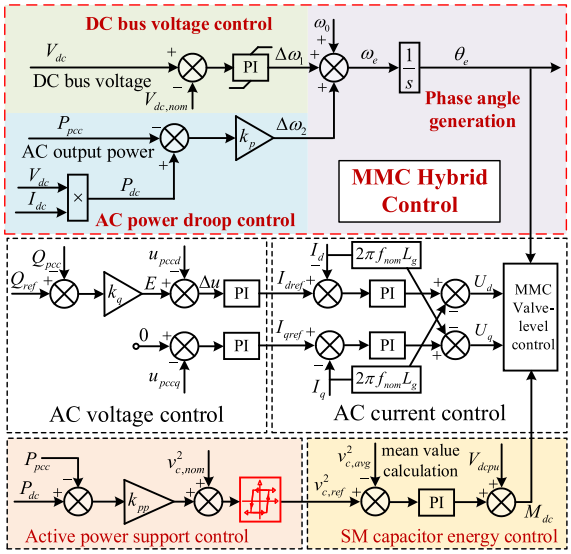

Fig. 6. Improved DGFM MMC transient stability enhanced control strategy.

III. Transient Stability Enhanced Control of DGFM MMC

The existing DGFM MMC control suffers from a transient stability issue under ac grid faults due to the coupling between power angle generation and SM capacitor voltage control. This article proposes a transient stability enhanced control method, which improves the power angle response speed while ensuring the active power support capability of MMC. The proposed control structure is shown in Fig. 6, which mainly includes a hybrid control branch for power angle θ_e generation and an active power support control branch for common-mode component $M_{\rm dc}$ generation.

The proposed control is mainly divided into five components: MMC hybrid control (power angle control), ac voltage control, ac control, active power support control, and SM capacitor energy control. In the active power support control, a limiter is added to prevent excessive support from the SM capacitors.

A. Hybrid Control for Power Angle Generation

The power angle of onshore MMC is generated through hybrid control, in which both ac power droop control (APC) and DVC aim to stabilize the dc bus voltage. This control mode enables the MMC power angle to directly control the dc bus voltage, allowing the MMC common-mode component $M_{\rm dc}$ to independently control the SM voltage. The hybrid control solves the problem of coupling power angle generation with SM capacitor voltage control in the existing DGFM MMC control.

The hybrid control aims to generate the power angle θ_e of DGFM MMC, which is a combination of APC and DVC. DVC employs a PI controller to regulate the deviation between the dc bus voltage and its reference, generating the control signal $\Delta\omega_1$. $P_{\rm pcc}$ and $P_{\rm dc}$ represent the output power at the PCC and the power fed into the dc bus. APC employs a power controller to regulate the deviation between $P_{\rm pcc}$ and $P_{\rm dc}$, generating the control signal $\Delta\omega_2$. $\Delta\omega_1$ and $\Delta\omega_2$ can be expressed as

$$\begin{cases}\Delta\omega_1 = k_{vp}(V_{\rm dc}-V_{\rm dc,nom}) + k_{vi}\int(V_{\rm dc}-V_{\rm dc,nom})dt \\ \Delta\omega_2 = k_p(P_{\rm dc}-P_{\rm pcc})\end{cases} \tag{3}$$

where k_{vp} and k_{vi} denote the proportional and integral control parameters of the DVC loop. $V_{\rm dc,nom}$ represents the reference value of the dc bus voltage. k_p is the proportional droop control parameter of active power.

According to (3), the angular frequency ω_e of DGFM MMC can be expressed as

$$\omega_e = \Delta\omega_1 + \Delta\omega_2 + \omega_0 \tag{4}$$

where ω_0 represents the reference angular frequency, generally equaling to the grid's rated angular frequency ω_g.

The reactive power droop control loop can be expressed as

$$E = k_q\left(Q_{\rm ref} - Q_e\right) + E_0 \tag{5}$$

where $k_{\rm q}$ represents the reactive power droop parameter, E_0 is the MMC reference voltage, $Q_{\rm ref}$ represents MMC reactive power setting value. In general, E_0 is set equal to the grid voltage U_g, $Q_{\rm ref}$ is set equal to 0.

B. Large-Signal Modeling of DGFM MMC With Proposed Hybrid Control

This subsection establishes a large signal model for DGFM MMC with hybrid control. The power angle can be used to calculate the output power $P_{\rm pcc}$ of the MMC system, and then the swing equation of the MMC system can be obtained.

By applying dq-axis decoupling in the voltage and current control loops to compensate for the filter inductance L_f, the PCC voltage $U_{\rm pcc}$ closely approximates the output of the reactive power droop control command $E_{\rm pcc}$.

As shown in Fig. 1, the active power $P_{\rm pcc}$ and reactive power $Q_{\rm pcc}$ at the PCC can be expressed as

$$\begin{cases}P_{\rm pcc} = \frac{3}{2}\frac{E_{\rm pcc}V_g}{X_g}\sin\delta \\ Q_{\rm pcc} = \frac{3}{2}\frac{E_{\rm pcc}^2 - E_{\rm pcc}V_g}{X_g}\cos\delta\end{cases} \tag{6}$$

where δ represents the power angle of the system, which is equal to the angle between the PCC voltage $E_{\rm pcc}$ and the grid voltage V_g. X_g denotes the grid impedance, calculated as $X_g = \omega_g L_g$, where ω_g is the angular frequency and L_g is the inductance of the grid.

By combining (5) and (6), the expression for the PCC voltage $E_{\rm pcc}$ can be further derived as follows:

$$E_{\rm pcc} = \frac{1}{3k_q}\left[\frac{3}{2}k_qV_g\cos\delta - X_g + A(\delta)\right] \tag{7}$$

where the simplified expression $A(\delta)$ can be expressed as

$$A(\delta) = \sqrt{\left(X_g - \frac{3}{2}k_qV_g\cos\delta\right)^2 + 6k_qX_g(E_0 + k_qQ_{\rm ref})}. \tag{8}$$

Combining (6) and (7), the relationship between the output power of the MMC and power angle can be formulated as

$$P_{\rm pcc}(\delta) = \frac{V_g}{2k_qX_g}\left[\frac{3}{2}k_qV_g\cos\delta - X_g + A(\delta)\right]\sin\delta. \tag{9}$$

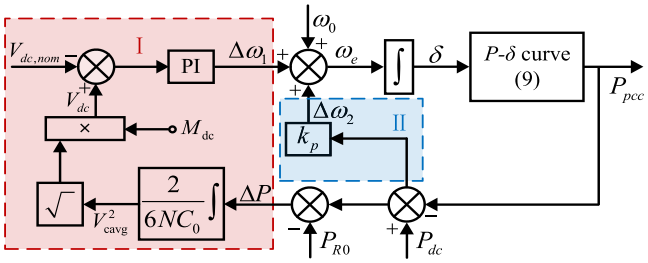

Fig. 7. Large signal model of DGFM MMC with proposed hybrid control.

The input power of the dc bus $P_{\rm dc}$ can be decomposed into three parts: the output power on ac side $P_{\rm pcc}$, the instantaneous power of SM capacitors $P_{c,}$ and the resistive losses on MMC arms P_{R0}. It can be expressed as follows:

$$\begin{cases} \int P_c dt = \frac{6NC_{\rm MMC}}{2}(v_{c,\rm avg}^2 - v_{c,\rm nom}^2) = \int (P_{\rm dc} - P_{\rm pcc} - P_{R0})dt \\ P_{R0} = 6[(\frac{I_{\rm dc}}{3})^2 + (\frac{P_{\rm pcc}}{2\sqrt{3}E_{\rm pcc}})^2]R_0 \end{cases} \tag{10}$$

where $v_{c,\rm nom}$ is the reference of the SM capacitor voltage.

Neglecting the influence of CCSC, the relationship among the dc bus voltage $V_{\rm dc}$, the average SM capacitor voltage $v_{c,\rm avg}$, and $M_{\rm dc}$ is expressed as

$$V_{\rm dc} = NM_{\rm dc}v_{c,\rm avg}. \tag{11}$$

Combining (1)–(11), the large signal model of DGFM MMC with the proposed hybrid control is shown in Fig. 7.

The time derivative of the MMC power angle δ, represented $\delta\bullet$, can be expressed as

$$\dot{\delta} = \omega_e - \omega_0. \tag{12}$$

The power angle swing equation is an important part of the MMC large signal model. It is shown by the following equation:

$$\ddot{\delta} = \dot{\omega}_{\rm e} = -k_p\dot{P}_{\rm pcc} + k_{vi}\left(V_{\rm dc} - V_{\rm dc,ref}\right) + k_{vp}\dot{V}_{\rm dc}. \tag{13}$$

Based on (6), the derivative of the output power $\rm P\bullet_{pcc}$ with respect to the power angle can be expressed as

$$\dot{P}_{\rm pcc} = \frac{3}{2}\frac{\dot{E}_{\rm pcc}\dot{\delta}V_g}{X_g}\sin\delta + \frac{3}{2}\frac{E_{\rm pcc}V_g}{X_g}\cos\delta\,\dot{\delta} \tag{14}$$

where the time derivative of the voltage $E_{\rm pcc}$ can be expressed as

$$\begin{aligned} \dot{E}_{\rm pcc} &= \frac{\partial E_{\rm pcc}}{\partial t} = \frac{\partial E_{\rm pcc}}{\partial \delta}\frac{\partial \delta}{\partial t} = \frac{\partial E_{\rm pcc}}{\partial \delta}\dot{\delta} \\ &= \frac{\dot{\delta}}{2k_q}\left[-k_qV_g\sin\delta + \frac{k_qV_g\sin\delta(\frac{2}{3}X_g - k_qV_g\cos\delta)}{A(\delta)}\right]. \end{aligned} \tag{15}$$

C. Transient Stability Analysis of DGFM MMC With Proposed Hybrid Control

When the voltage or frequency of the ac grid drops, the system power will fluctuate with the change of the power angle of the MMC. If the power angle fluctuates too much and cannot stabilize at the equilibrium point, MMC will lose stability.

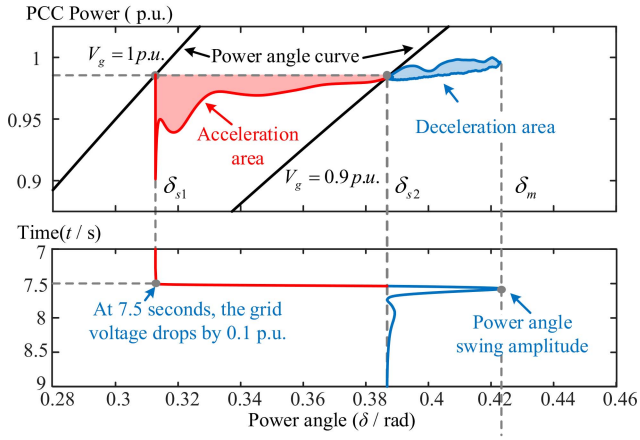

Fig. 8. δ-P-t variation diagram under grid voltage fault.

Fig. 8 depicts the characteristics of power angle varying with active power and time (δ-P-t) during an ac voltage fault, where the grid voltage drops from 1.0 to 0.9 p.u.. The two black oblique lines in Fig. 8 are the MMC power angle curve under different grid voltages (viz. V_g = 1 p.u. and V_g = 0.9 p.u.). They are obtained based on (9). The values of $\delta_{\rm s1}$ and $\delta_{\rm s2}$ can be calculated by setting the output power of (9) to 1 p.u.

During the change of operation point, the transition curve of MMC can be divided into a red AA and a blue DA, where the power angle range of the red AA is δ_{s1}–δ_{s2}; the power angle range of the blue DA is δ_{s2}–δ_m. As shown in the power angle-time diagram below, the duration in the AA is significantly shorter than that in the DA. Thus, the absolute value of the MMC power angle change rate $|\omega$-$\omega_0|$ is nonconstant: it is larger in the AA and smaller in the DA.

Compared with the power angle curve in Fig. 4(a), the power angle curve with the proposed hybrid control in Fig. 8 has a smaller AA and a smaller power angle overshoot δ_m in the DA. This makes the MMC with hybrid control have better transient stability than the existing DGFM control under grid voltage fault.

Fig. 9 shows the δ-f-t variation curve under ac grid frequency fault. When the grid frequency drops, its operation point transitions from the prefault operation point $\delta_{\rm s1}$ to the postfault operation point $\delta_{\rm s2}$. The power angle of MMC with the proposed hybrid control will respond quickly, reduce the power angle overshoot, reduce the minimum frequency drop, and improve system transient stability.

Fig. 10 displays a phase plane diagram comparing the proposed hybrid control and the existing DGFM control. Both grid frequency and voltage drop conditions are focused on. As illustrated in Fig. 10(a), the proposed hybrid control outperforms the existing DGFM control during voltage drops, exhibiting enhanced power angle stability under such disturbances. Similarly, Fig. 10(b) highlights the superior performance of the proposed hybrid control during frequency drops, maintaining stronger power angle stability compared to the existing strategy.

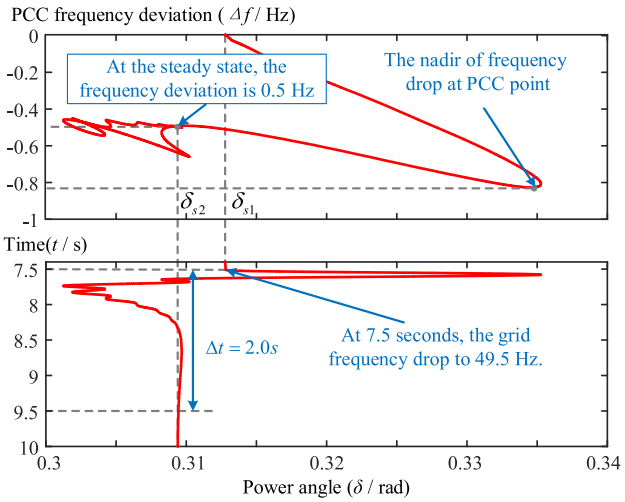

Fig. 9. δ-f-t variation diagram under grid frequency fault.

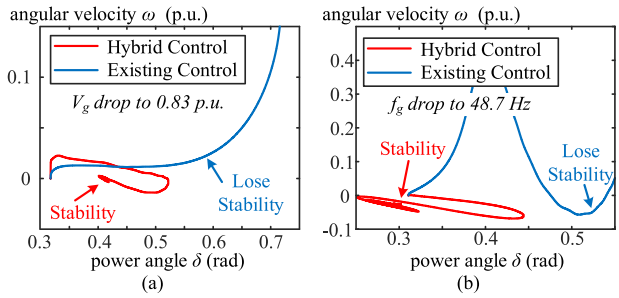

Fig. 10. Phase plane diagram of different control methods under grid fault. (a) V_g drop phase Plane plot. (b) f_g drop phase plane plot.

In summary, integrating the APC and DVC into a unified control branch allows the power angle to respond more rapidly to grid faults while reducing power angle overshoot. This helps improve the transient stability of the onshore MMC.

D. Active Power Support Control for Common-Mode Component Generation

In this article, the power angle generation branch is fully utilized to improve the transient stability of the DGFM MMC under ac faults. Rapid response and less overshoot of the power angle is realized during a fault. Additionally, in order to support sufficient active support capability to the grid, this section proposes an ac active support control based on the common-mode component generation branch. This method enables independent voltage control and active ac power support. The control block diagram for this approach is shown in Fig. 6.

Fig. 6 illustrates that the common-mode component $M_{\rm dc}$ control branch comprises two functional modules: 1) SM capacitor energy control and 2) ac active power support. The mathematical representation of the $M_{\rm dc}$ control branch can be expressed as

$$M_{\rm dc} = k_{p,{\rm mdc}}[v_{c,{\rm avg}}^2 - v_{c,{\rm nom}}^2 + k_{\rm pp}(P_{\rm pcc} - P_{\rm dc})]$$

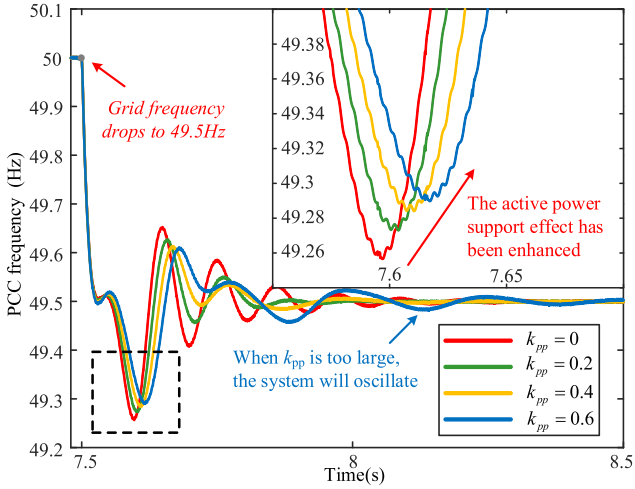

Fig. 11. AC power active power support control effect.

$$+ k_{i,{\rm mdc}} \int [v_{c,{\rm avg}}^2 - v_{c,{\rm nom}}^2 + k_{\rm pp}(P_{\rm pcc} - P_{\rm dc})]dt \tag{16}$$

where parameters $k_{p,{\rm mdc}}$ and $k_{i,{\rm mdc}}$ represent the proportional and integral parameters for the independent control of MMC SM energy, while $k_{\rm pp}$ represents the active power support parameter for ac systems. By regulation of $V_{c,{\rm nom}}$, the SM capacitor voltage can be controlled independently while maintaining the dc bus voltage stability.

AC grid fault will cause energy imbalance between ac and dc side. In this case, the active power support scheme can autonomously absorb or release energy through the MMC SM capacitors, providing support to the ac grid.

In Fig. 11, the PCC frequency changes when the MMC active power support parameter increases from 0 to 0.6. Increasing the active power support parameter improves the PCC frequency nadir, but an excessively large $k_{\rm pp}$ will induce transient oscillations.

IV. Parameter Tuning of the Proposed Transient Stability Enhanced Control

This section proposes an optimal parameter tuning method for the proposed transient stability enhanced control. By linearizing the fourth-order differential equations, the system's Jacobian matrix is derived. This is followed by a root locus analysis of its transfer function to enable optimal parameter tuning. The active power support parameter $k_{\rm pp}$ is used as an example to demonstrate the method's effectiveness in enhancing transient stability and active power support.

A. Linearization Modeling of DGFM MMC Considering Transient Stability Enhanced Control

Based on the analysis in Section III, the fourth-order large signal model of the DGFM MMC is derived as follow.

According to the dc voltage (11), the time derivative expression of the $V_{\rm dc}$ can be derived as follow:

$$\dot{V}_{\rm dc} = N^2 M_{\rm dc}^2 \frac{P_{\rm dc} - P_{\rm pcc} - P_{R0}}{6NC_{\rm MMC}V_{\rm dc}} + \frac{V_{\rm dc}}{M_{\rm dc}}\dot{M}_{\rm dc}. \tag{17}$$

The time derivative of the common-mode component $M_{\rm dc}$, represented by $\mathrm{M}\bullet_{\rm dc}$, can be expressed as (18), shown at the bottom of this page.

Combining (12), (13), (17), and (18), a fourth-order differential equation can be obtained in (19), shown at the bottom of this page. which is expressed in terms of (δ, ω_e-ω_0, V_{dc}, $M_{\rm dc}$) (at the bottom of the next page)

It needs to point out that this article primarily studies the transient stability issue of DFGM MMC under shallow ac grid faults. In this scenario, the current saturation will not be triggered during fault. Therefore, the current limiting control is not considered in establishing the large signal model.

The nonlinear large signal model can be linearized at the steady-state equilibrium point, and the steady-state equilibrium point equation of the system is shown as

$$\begin{cases} \delta(\dot{\delta} = 0) \\ \omega_0 = \omega_g(\delta\omega_1 = 0, \delta\omega_2 = 0) \\ V_{dc,0} = V_{dc,nom}(\dot{V}_{dc} = 0) \\ M_{dc,0} = \frac{V_{dc,nom}}{NV_{c,nom}} \end{cases} \tag{20}$$

where δ_0 is the system steady-state power angle obtained from the power angle curve (9). ω_0 is the initial value of the angular velocity, $V_{\rm dc,0}$ is the initial value of the dc bus voltage, $M_{\rm dc,0}$ is initial value of the MMC common-mode component.

Taking the steady-state equilibrium point of (20) as the initial value of the system ($\boldsymbol{x}_0 = [\delta_0\ \omega_0\ V_{\rm dc,0}\ M_{\rm dc,0}]^{\rm T}$), and linearizing the fourth-order large-signal model at $\boldsymbol{x}_0$. The Jacobian matrix of the linearized model can be obtained as

$$J(x_0) = \begin{bmatrix} 0 & 1 & 0 & 0 \\ k_{vp}A_{31} & A_{22} & k_{vi} + k_{vp}A_{33} & k_{vp}A_{34} \\ A_{31} & A_{32} & A_{33} & A_{34} \\ A_{41} & A_{42} & 2k_{i,mdc}M_{dc}^{-2}V_{dc} & -2k_{i,mdc}M_{dc}^{-3}V_{dc}^2 \end{bmatrix}. \tag{21}$$

The parameters in the Jacobian matrix are as follows:

$$\begin{aligned} A_{22} =& -k_p[1.5\dot{E}_{pcc}(\delta)V_g\sin\delta + 1.5E_{pcc}(\delta)V_g\cos\delta]/X_g \\ &+ k_{vp}A_{32} \\ A_{31} =& \frac{-N^2M_{dc}^2\dot{P}_{pcc}}{6NC_{MMC}V_{dc}}(N^2 + 2k_{\rm p,mdc}M_{dc}^{-3}V_{dc}^2) \\ &+ k_{\rm i,mdc}k_{pp}N^2M_{dc}^{-1}V_{dc}\dot{P}_{pcc} \\ A_{32} =& N^2M_{dc}^{-1}V_{dc}k_{\rm p,mdc}k_{pp}\dot{P}_{pcc} \\ A_{33} =& 3k_{\rm i,mdc}M_{dc}^{-3}V_{dc}^2 - k_{\rm i,mdc}N^2V_{c,nom}^2M_{dc}^{-1} \\ A_{34} =& -3k_{\rm i,mdc}M_{dc}^{-4}V_{dc}^3 + k_{\rm i,mdc}N^2V_{c,nom}^2V_{dc}M_{dc}^{-2} \\ A_{41} =& k_{\rm i,mdc}k_{pp}N^2\dot{P}_{pcc} - k_{\rm p,mdc}N^2\dot{P}_{pcc}/3NC_{MMC}. \end{aligned} \tag{22}$$

Based on (20)–(22), the system's state-space equation can be derived. Furthermore, the transfer function of the DGFM MMC system is shown as

$$G(s) = \boldsymbol{C}[s\boldsymbol{I} - J(\boldsymbol{x}_0)]^{-1}\boldsymbol{x}_0 \tag{23}$$

where $\boldsymbol{I}$ is the 4∗4 identity matrix. $\boldsymbol{C}$ is the system output matrix, $\boldsymbol{C}$ = [1,0,0,0], take δ as the system output.

The denominator of G(s) can be solved for poles, and the numerator can be solved for zeros.

B. Root Locus-Based Parameter Tuning

Section IV-A derives the linearized model and transfer function of the DGFM MMC system. Fig. 12 illustrates the system oscillation problem caused by excessive active support parameter when the grid frequency drops. Therefore, this section takes the grid frequency drop fault as an example to tuning the MMC active support control parameter $k_{\rm pp}$. Consequently, the root locus diagram is systematically plotted with respect to different active power support parameter $k_{\rm pp}$, which is shown in Fig. 12.

Fig. 12 shows the root locus of DGFM MMC with the variation of active power support parameter $k_{\rm pp}$ from 0 to 1.4. The DGFM MMC system exhibits four poles and three zeros in its transfer function.

In Fig. 12, the first zero appears in close proximity to the first pole, and similarly, the second zero neighbors the second pole. The system demonstrates zero-pole cancellation effects, resulting in the first pole and the second pole having minimal

$$\dot{M}_{\rm dc} = \frac{k_{\rm i,mdc}[M_{\rm dc}^{-2}V_{\rm dc} - N^2V_{c,\rm nom}^2 + k_{\rm pp}N^2(P_{\rm pcc} - P_{\rm dc})] + N^2k_{\rm p,mdc}k_{\rm pp}\dot{P}_{\rm pcc} + 2k_{\rm p,mdc}M_{\rm dc}^{-2}V_{\rm dc}\dot{V}_{\rm dc}}{N^2 + 2k_{\rm p,mdc}M_{\rm dc}^{-3}V_{\rm dc}^2}. \tag{18}$$

$$\begin{cases} \dot{\delta} = \omega - \omega_0 \\ \dot{\omega} = \Delta\dot{\omega}_1 + \Delta\dot{\omega}_2 = -k_p\dot{P}_{\rm pcc} + k_{vi}(V_{\rm dc} - V_{\rm dc,nom}) + k_{vp}\dot{V}_{\rm dc} \\ \dot{V}_{\rm dc} = \Big\{N^2M_{\rm dc}^2\frac{P_{\rm dc} - P_{\rm pcc} - P_{R0}}{6NC_{\rm MMC}V_{\rm dc}}(N^2 + 2k_{\rm p,mdc}M_{\rm dc}^{-3}V_{\rm dc}^2) + k_{\rm i,mdc}[M_{\rm dc}^{-3}V_{\rm dc}^3 - N^2V_{c.\rm nom}^2M_{\rm dc}^{-1}V_{\rm dc} + k_{\rm pp}N^2M_{\rm dc}^{-1}V_{\rm dc}(P_{\rm pcc} - P_{\rm dc})] \\ + N^2M_{\rm dc}^{-1}V_{\rm dc}k_{\rm p,mdc}k_{\rm pp}\dot{P}_{\rm pcc}\Big\} \\ \dot{M}_{\rm dc} = k_{\rm i,mdc}[M_{\rm dc}^{-2}V_{\rm dc}^2 - N^2V_{c,\rm nom}^2 + k_{\rm pp}N^2(P_{\rm pcc} - P_{\rm dc})] + N^2k_{\rm p,mdc}k_{\rm pp}\dot{P}_{\rm pcc} + 2k_{\rm p,mdc}N^2(P_{\rm dc} - P_{\rm pcc} - P_{R0})/6NC_{\rm MMC} \end{cases} \tag{19}$$

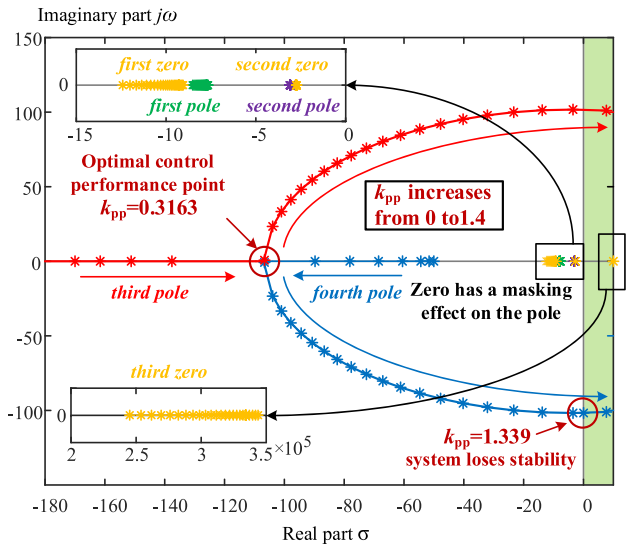

Fig. 12. Root locus curve with respect to different active power support coefficient k_{pp}.

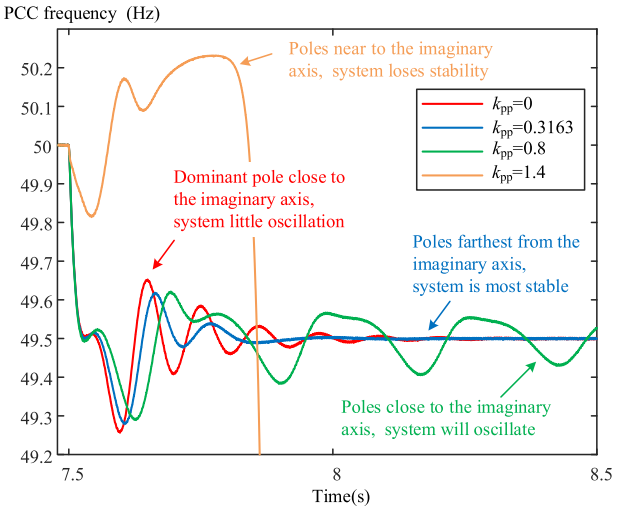

Fig. 13. PCC frequency response curve under different k_{pp}.

influence on the overall system response. This phenomenon persists even though these pole-zero pairs are relatively close to the imaginary axis.

As the value of k_{pp} increases, the third pole progressively moves closer to the imaginary axis, while the fourth pole simultaneously shifts away from it. When k_{pp} is below 0.3163, higher values of k_{pp} enhance the system damping, thereby improving the transient stability of the system. However, if k_{pp} exceeds 0.3163, both the third and fourth poles begin to approach the imaginary axis, reducing transient stability and inducing system oscillations. Once k_{pp} surpasses 1.339, the system becomes unstable, with the third and fourth poles crossing the imaginary axis.

Fig. 13 illustrates the frequency response curve of the PCC point under different k_{pp} values. At 7.5 s, the grid frequency drops to 49.5 Hz. When $k_{pp} = 0$, the system lacks active power support, resulting in the most significant frequency drop, accompanied by oscillations and a prolonged stabilization period. With $k_{pp} = 0.3163$, the system's dominant characteristic root is farthest from the imaginary axis, providing active power support while achieving the fastest convergence. This ensures optimal transient stability. At $k_{pp} = 0.8$, the active power support improves slightly compared to $k_{pp} = 0.3163$. However, the characteristic root moves closer to the imaginary axis, causing increased oscillations and reduced transient stability. When $k_{pp} = 1.4$, the characteristic root shifts to the right half of the complex plane, leading to system instability due to its unfavorable position.

The proposed root locus-based parameter tuning method can be used to optimally select specific control parameters, which is helpful for the enhancement of transient stability and improvement of grid frequency support capacity.

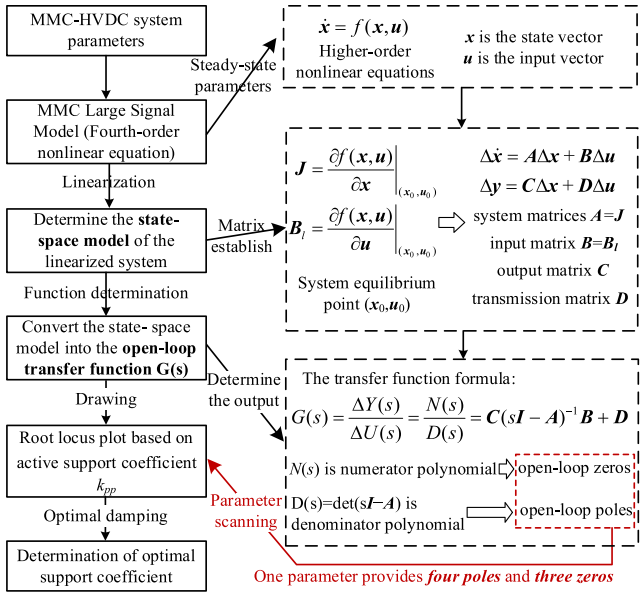

Fig. 14. Parameter tuning flowchart.

C. Parameter Tuning Flowchart

The parameter tuning process can be summarized into the following parameter tuning flowchart.

As shown in Fig. 14, the parameter tuning flowchart of the proposed transient stability enhanced control contains four steps:

1) By substituting the parameters of the MMC-HVDC system into the large-signal model, the fourth-order nonlinear equations for the MMC-HVDC are derived.
2) Derive the state-space equations of the MMC-HVDC system by linearizing the large-signal model.
3) Calculate the open-loop transfer function G(s) of the system based on the system's state-space equations.
4) Plot root locus for the active support coefficient k_{pp} based on the open-loop transfer function of the system. By identifying the optimal damping characteristic roots on the root locus, the transient stability optimization of the MMC-HVDC system can be achieved.

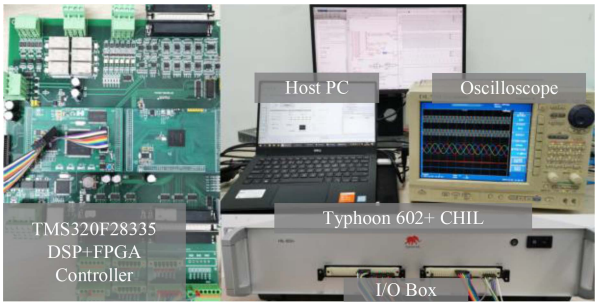

Fig. 15. CHIL experimental hardware platform.

TABLE I
MMC PARAMETERS

Parameters	Symbols	Values
DC input power/system power base	P_{dc}/ S_{base}	1000 MW
DC bus voltage	V_{dc}	500 kV
Grid voltage/AC voltage base	U_g/ V_{base}	260 kV(rms)
SM capacitor	C_{MMC}	6 mF
Per arm SMs	N	400
Arm resistor	R_0	0.2 Ω
Arm inductance	L_0	40 mH
MMC filter inductance	L_f	1 mH
Grid inductance	L_g	65 mH
Impedance base	Z_{base}	67.6 Ω

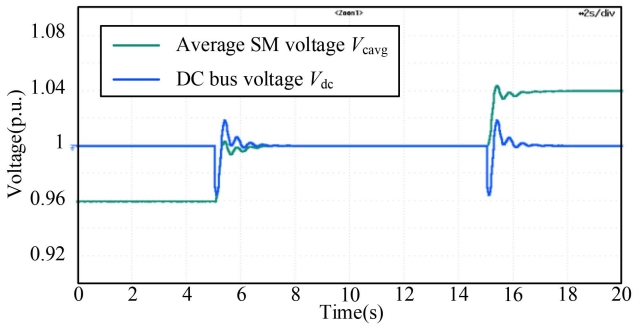

Fig. 16. Decoupling of DC voltage and SM capacitor voltage under the proposed transient stability enhanced control.

V. EXPERIMENTAL VERIFICATION

To verify the proposed active power support method, a CHIL experimental platform is developed. As shown in Fig. 15, the proposed control strategy is simulated in real-time using the Typhoon 602+ simulator with a time step of 1 μs. The MMC control algorithm is implemented on a TMS320F28335 digital signal processor integrated with a Spartan6 XC6SLX16 FPGA. Real-time interaction between the Typhoon 602+ simulator and the controller is established through the exchange of both digital signals and analog signals. The parameters of the DGFM MMC are shown in Table I.

When the onshore grid frequency drops, the active power support control uses the energy of the SM capacitor to support the grid. In Fig. 16, the dc bus voltage $V_{\rm dc}$ is controlled unchanged, and the SM voltages of the MMC are adjusted independently, verifying the effectiveness of the capacitor voltage decoupling control.

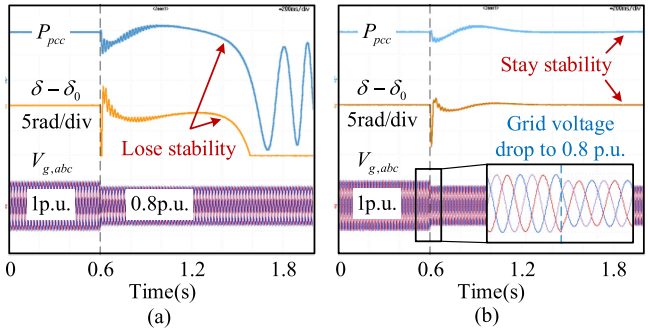

Fig. 17. Comparison of transient stability under power grid voltage drop. (a) Existing control. (b) Proposed transient stability enhanced control.

The SM capacitor voltage decoupling control effect of Fig. 16, which proves that the proposed control method has the SM voltage decoupling control capability.

The comparison between the existing DGFM MMC control and the proposed transient stability enhanced control under grid voltage drop is shown in Fig. 17. When the grid voltage drops to 0.8 p.u. at 0.6 s, it causes a power imbalance between the ac and dc sides. The existing control method loses transient stability, while the proposed control method maintains synchronization with the grid. This demonstrates that the proposed control method exhibits better transient stability during grid voltage drop.

According to the analysis in Section III, the proposed control method has active power support capability. By utilizing the SM energy, the stability of the MMC system can be improved when the ac grid frequency decreases, and at the same time raise the lowest point of the PCC frequency.

Fig. 18 shows the waveforms of the frequency f_g, output power $P_{\rm pcc}$, and ac at the PCC during a sudden grid frequency drop. Fig. 18(a) presents the PCC waveforms under the existing control, while Fig. 18(b) shows the PCC waveforms under the proposed transient stability enhanced control.

Fig. 18(a) and (b) show that the proposed control method can increase the PCC minimum frequency from 48.308 to 48.478 Hz during the period when the grid frequency drops from 50 to 49 Hz. Furthermore, the power waveforms in Fig. 18(a) show that with the proposed transient stability enhanced control, the MMC system achieves: 1) a 34.4% reduction in settling time (from 2.50 to 1.64 s), and 2) a 64.7% suppression of active power overshoot (from 0.527 to 0.186 p.u.). These results confirm that the MMC's ac power active power support control effectively mitigates frequency deviations while simultaneously improving transient stability through faster response and reduced power overshoot.

According to the analysis in Section IV, when the active power support parameter of ac power is too large, the MMC system may oscillate or even become unstable when the frequency decreases. Therefore, the comparison of the frequency waveform

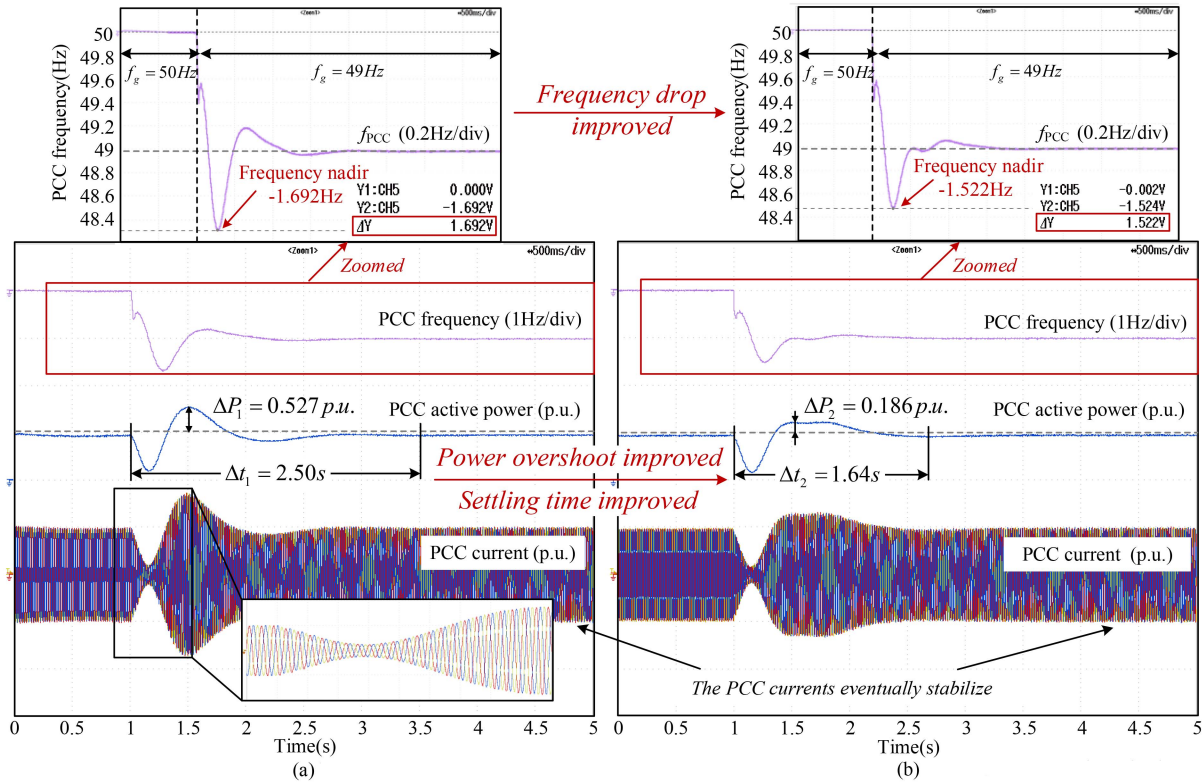

Fig. 18. Comparison of grid frequency drop with and without power support. (a) Existing control method. (b) Proposed transient stability enhanced control

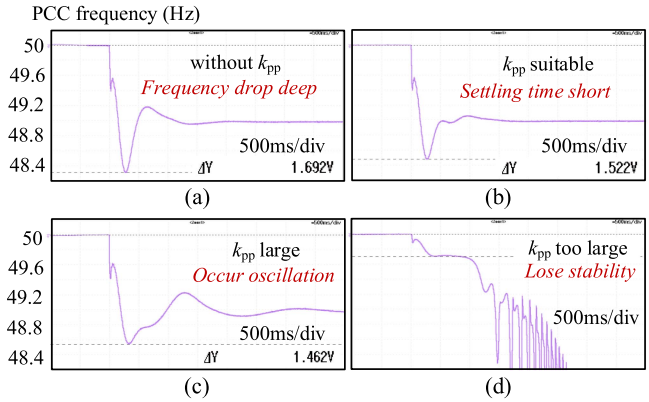

Fig. 19. PCC frequency waveform under different AC power active power support parameters. (a) $k_{pp} = 0$. (b) $k_{pp} = 0.31$. (c) $k_{pp} = 0.8$. (d) $k_{pp} = 1.3$.

of PCC under different ac power supply active power support coefficients is shown in Fig. 19.

The frequency response under different k_{pp} is shown in Fig. 19. As observed in Fig. 19(a) and (b), increasing the active power support coefficient k_{pp} from 0 to 0.31 effectively reduces both the maximum frequency deviation during disturbances and the system's settling time. However, a comparison between Fig. 19(b) and (c) reveals that while higher k_{pp} values continue to decrease frequency deviations, they simultaneously introduce system oscillations and significantly prolong the settling time. Moreover, as shown in Fig. 19(c) and (d), further increasing the k_{pp} will lead to system instability.

The ac power active power support control can actively release the MMC SM voltage to support the grid frequency. Both simulation and experimental results show that the tuning of the control parameter will influence the active power support capacity and transient stability of the system. The root locus-based parameter turning method in Section IV can be used to select the optimal parameters to achieve the optimal MMC control effect.

In summary, compared to the existing methods [18], an additional power feedforward term is added to the power-angle generation branch in the proposed control strategy, which effectively enhances the power-angle response during faults and significantly improves transient stability. Furthermore, the decoupling method is improved so that the SM capacitor can be controlled independently of the system power angle. This allows the SM capacitor to provide autonomous support, thereby enhancing the active support capacity to the ac grid.

VI. Conclusion

To enhance transient stability during ac grid faults while maintaining support capability. This article proposes a transient stability enhanced control for DGFM MMC. The proposed method consists of two key branches: a hybrid control branch for power angle generation and an active power support control branch for common-mode component generation. The main conclusions drawn are as follows.

1) To enhance the transient stability of DGFM MMC under ac grid faults, an APC and DVC hybrid control branch is proposed for the generation of power angle. By increasing

the power angle response speed and reducing overshoot, the transient stability of MMC is improved

2) To improve the active support capacity on the premise of transient stability enhancement, an active power support control branch is further proposed for the generation of common-mode component. By decoupling the dc bus and SM capacitor voltage, the active support to the ac grid is guaranteed with the proposed common-mode component generation branch.
3) To enhance the performance of the proposed control strategy, a control parameter tuning method based on root locus analysis is presented. This method enables the optimal combination of transient stability and active support capability for the DGFM MMC.

REFERENCES

[1] S. Zhang, B. Hu, X. Huang, D. Sun, H. Nian, and Y. Fan, "Active power transfer capability enhancement for DFIG-based WT under asymmetrical faults," *IEEE Trans. Power Electron.*, vol. 40, no. 10, pp. 14313–14317, Oct. 2025.

[2] F. Yang et al., "Multi-dimensional assessment of decarbonization technologies and pathways in China's iron and steel industry: An energy-process chain perspective," *Energy Strategy Rev.*, vol. 61, 2025, Art. no. 101810.

[3] S. Zhang, B. Hu, Y. Qiu, B. Hua, D. Sun, and H. Nian, "Asymmetrical fault ride-through enhancement for DFIG-based WT based on sequence coupling analysis," *IEEE Trans. Ind. Electron.*, to be published, doi: 10.1109/TIE.2025.3605460.

[4] Z. He, J. Hu, L. Lin, P. Zeng, and L. Hang, "A generalized dc asymmetrical fault analysis method for MMC-HVDC grids considering metallic return conductors," *IEEE Trans. Power Del.*, vol. 39, no. 5, pp. 2568–2579, Oct. 2024.

[5] L. Fernández, "Global capacity of offshore wind power 2009-2024," *Statista*, 2025. [Online]. Available: https://www.statista.com/statistics/476327/global-capacity-ofoffshore-wind-energy/

[6] Z. He, M. Lu, L. Hang, P. Zeng, and Y. Liu, "Capacitor voltage imbalance mechanism and balancing control of MMC when riding through PTG fault," *CSEE J. Power Energy Syst.*, vol. 10, no. 2, pp. 778–785, Mar. 2024.

[7] M. A. Perez, S. Bernet, J. Rodriguez, S. Kouro, and R. Lizana, "Circuit topologies, modeling, control schemes, and applications of modular multilevel converters," *IEEE Trans. Power Electron.*, vol. 30, no. 1, pp. 4–17, Jan. 2015.

[8] G. Li and J. Liang, "Modular multilevel converters: Recent applications [history]," *IEEE Electrific. Mag.*, vol. 10, no. 3, pp. 85–92, Sep. 2022.

[9] National Grid ESO, "Appendices to the technical report on the events of 9 August 2019," Sep. 2019. [Online]. Available: https://www.ofgem.gov.uk/sites/default/files/docs/2019/09/eso_technical_report_-_appendices_-_final.pdf

[10] Australian Energy Regulator (AER) "The black system event compliance report: Investigation into the pre-event, system restoration, and market suspension aspects surrounding the 28 September 2016 Event," AER, Adelaide, Australia, 2018. [Online]. Available: https://www.aer.gov.au/system/files/Black%20System%20Event%20Compliance%20Report%20-%20Investigation%20into%20the%20Pre-event%20System%20Restoration%20and%20Market%20Suspension%20aspects%20surrounding%20the%2028%20September%202016%20event.pdf

[11] C. Wu, Z. Zou, X. Xiong, Y. Wang, and F. Blaabjerg, "Fast active power recovery for grid-forming converter during postfault under different R/X ratios of grid impedance," *IEEE Trans. Ind. Electron.*, vol. 72, no. 10, pp. 10130–10140, Oct. 2025.

[12] L. Zhan, B. Hu, L. Chen, Y. Liao, M. Li, and H. Nian, "Transient stability enhancement of current limited-GFM inverters based on varying virtual impedance," *IEEE Trans. Ind. Electron.*, vol. 71, no. 12, pp. 15946–15958, Dec. 2024.

[13] T. Huang, S. L. Voronca, A. A. Purcarea, A. Estebsari, and E. Bompard, "Analysis of chain of events in major historic power outages," *Adv. Elect. Comput. Eng.*, vol. 14, no. 3, pp. 63–70, 2014.

[14] Q. Shi et al., "Grid strength assessment method for evaluating small-signal synchronization stability of grid-following and grid-forming converters integrated systems," *J. Modern Power Syst. Clean Energy*, vol. 13, no. 1, pp. 55–65, 2025.

[15] R. Pan, D. Liu, S. Liu, J. Yang, L. Kou, and G. Tang, "Stability comparison between grid-forming and grid-following based wind farms integrated MMC-HVDC," *J. Modern Power Syst. Clean Energy*, vol. 11, no. 4, pp. 1341–1355, 2022.

[16] J. Yan, X. Shi, T. Liu, Z. Wang, L. Zhang, and L. Lin, "Weak grid characteristic analysis and operating mode selection for voltage support enhancement of wind farms connected to MMC-HVDC during asymmetric faults," *IEEE Trans. Power Electron.*, vol. 41, no. 2, pp. 2629–2647, Feb. 2026, doi: 10.1109/TPEL.2025.3613420.

[17] S. Samimi, F. Gruson, P. Delarue, F. Colas, M. M. Belhaouane, and X. Guillaud, "MMC stored energy participation to the dc bus voltage control in an HVDC link," *IEEE Trans. Power Del.*, vol. 31, no. 4, pp. 1710–1718, Aug. 2016.

[18] H. W. Jiang, G. Li, Y. Xin, L. Wang, and Y. Xu, "A novel coordinated control strategy for frequency regulation of MMC-HVDC connecting offshore wind farms," *IEEE Trans. Sustain. Energy*, vol. 15, no. 2, pp. 1028–1038, Apr. 2024.

[19] H. Kim et al., "Exploiting redundant energy of MMC–HVDC to enhance frequency response of low inertia AC grid," *IEEE Access*, vol. 7, pp. 138485–138494, 2019.

[20] H. Zhang, W. Xiang, and J. Wen, "Dual grid-forming control with energy regulation capability of MMC-HVDC system integrating offshore wind farms and weak grids," *IEEE Trans. Power Syst.*, vol. 39, no. 1, pp. 261–272, Jan. 2024.

[21] H. Zhang, W. Xiang, Y. He, and J. Wen, "Optimal energy utilization of MMC-HVDC system integrating offshore wind farms for onshore weak grid inertia support," *IEEE Trans. Power Syst.*, vol. 39, no. 1, pp. 1304–1318, Jan. 2024.

[22] Y. Huang, X. Yuan, J. Hu, P. Zhou, and D. Wang, "DC-bus voltage control stability affected by AC-bus voltage control in VSCs connected to weak AC grids," *IEEE J. Emerg. Sel. Topics Power Electron.*, vol. 4, no. 2, pp. 445–458, Jun. 2016.

[23] L. Shen, M. Barnes, R. Preece, J. V. Milanovic, K. Bell, and M. Belivanis, "The effect of VSC-HVDC control on ac system electromechanical oscillations and DC system dynamics," *IEEE Trans. Power Del.*, vol. 31, no. 3, pp. 1085–1095, Jun. 2016.

[24] A. Poulose and S. Kim, "Transient stability analysis and enhancement techniques of renewable-rich power grids," *Energies*, vol. 16, no. 5, Jan. 2023, Art. no. 2495, doi:10.3390/en16052495.

[25] P. Sun, Z. Tian, M. Huang, X. Zha, P. Feng, and X. Ma, "Power supporting control of grid-forming converters under grid voltage sags for transient stability enhancement and overcurrent limitation," *IEEE J. Emerg. Sel. Topics Power Electron.*, vol. 13, no. 1, pp. 626–636, Feb. 2025.

[26] H. Zhou, W. Yao, M. Zhou, X. Ai, J. Wen, and S. Cheng, "Active energy control for enhancing AC fault ride-through capability of MMC-HVDC connected with offshore wind farms," *IEEE Trans. Power Syst.*, vol. 38, no. 3, pp. 2705–2718, May 2023, doi: 10.1109/TPWRS.2022.3179443.

[27] K. Sun, H. Zhou, W. Yao, B. Xiao, and J. Wen, "Comprehensive control of MMC-HVDC integrated offshore wind farm system including optimized energy control for fast frequency support," *J. Modern Power Syst. Clean Energy*, to be published, doi: 10.35833/MPCE.2024.000975.